REPORT

OPTICS

Observation of bulk Fermi arc and polarization half charge from paired exceptional points

Hengyun Zhou,[1]*† Chao Peng,[1,2]* Yoseob Yoon,[3] Chia Wei Hsu,[4] Keith A. Nelson,[3] Liang Fu,[1] John D. Joannopoulos,[1] Marin Soljačić,[1] Bo Zhen[5]‡

The ideas of topology have found tremendous success in closed physical systems, but even richer properties exist in the more general open or dissipative framework. We theoretically propose and experimentally demonstrate a bulk Fermi arc that develops from non-Hermitian radiative losses in an open system of photonic crystal slabs. Moreover, we discover half-integer topological charges in the polarization of far-field radiation around the bulk Fermi arc. Both phenomena are shown to be direct consequences of the non-Hermitian topological properties of exceptional points, where resonances coincide in their frequencies and linewidths. Our work connects the fields of topological photonics, non-Hermitian physics, and singular optics, providing a framework to explore more complex non-Hermitian topological systems.

In recent years, topological effects have been widely explored in closed and lossless systems, where the physics is characterized by a Hermitian operator that ensures a real energy spectrum and a complete, orthogonal set of eigenfunctions. This has revealed a number of previously unknown phenomena such as topologically nontrivial band structures (*1*, *2*), and promising applications including backscattering-immune transport (*3*–*5*). However, most systems, particularly in photonics, are generically non-Hermitian because of radiation into open space or material gain or loss. Non-Hermiticity enables even richer topological properties, often with no counterpart in Hermitian frameworks (*6*–*8*). One such example is the emergence of a new class of degeneracies, commonly referred to as exceptional points (EPs), where two or more resonances of a system coalesce in both eigenvalues and eigenfunctions (*9*). So far, isolated EPs in parameter space (*10*–*12*) and continuous rings of EPs in momentum space (*13*) have been studied across different wave systems because of their intriguing properties, such as unconventional transmission or reflection (*14*) and relations to parity-time symmetry (*15*), as well as their unique applications in sensing (*16*, *17*) and single-mode lasing (*18*, *19*).

We theoretically design and experimentally realize a new configuration of isolated EP pairs in momentum space, which allows us to reveal topological signatures of EPs in the band structure and far-field polarization, and to extend topological band theory into the realm of non-Hermitian systems. Specifically, we demonstrate that a Dirac point (DP) with nontrivial Berry phase can split into a pair of EPs (*20*–*22*) when radiation loss—a form of non-Hermiticity—is added to a two-dimensional (2D)–periodic photonic crystal (PhC) structure. The EP-pair generates a distinct double–Riemann sheet topology in the complex band structure, which leads to two notable consequences: bulk Fermi arcs and polarization half topological charges. First, we demonstrate that this pair of EPs is connected by an open-ended isofrequency contour—a bulk Fermi arc—in direct contrast to the common intuition that isofrequency contours are necessarily closed loops. The bulk Fermi arc here is a special topological signature of non-Hermitian effects in paired EPs and resides in the bulk dispersion of a 2D system. This is fundamentally different from the previously known surface Fermi arcs that arise from the 2D projection of Weyl points in 3D Hermitian systems. Moreover, we find experimentally that around the Fermi arc, the far-field polarization of the system exhibits a robust half-integer winding number (*23*–*25*), analogous to the orientation reversal on a Möbius strip. We show that this is a direct consequence of the topological band-switching properties across the Fermi arc connecting the EP pair and is direct experimental proof of the $\nu = \pm 1/2$ topological index associated with an EP (*8*). With comprehensive comparisons between analytical models, numerical simulations, and experimental measurements, our results are a direct validation of non-Hermitian topological band theory and present its novel application to the field of singular optics.

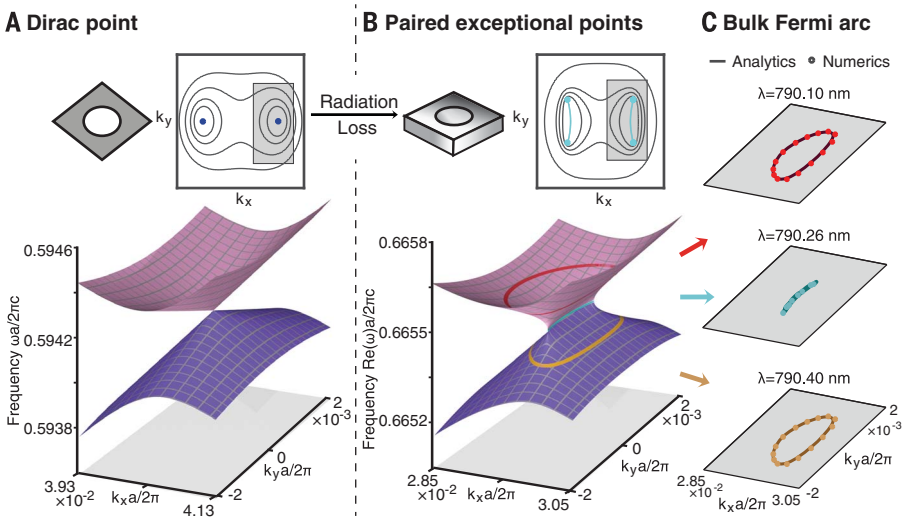

Fig. 1. Bulk Fermi arc arising from paired exceptional points split from a single Dirac point. (**A** and **B**) Illustration of photonic crystal (PhC) structures, isofrequency contours, and band structures. (A) Band structure of a 2D-periodic PhC consisting of a rhombic lattice of elliptical air holes, featuring a single Dirac point on the positive k_x axis. (B) The real part of the eigenvalues of an open system consisting of a 2D-periodic PhC slab with finite thickness, where resonances experience radiation loss. The Dirac point splits into a pair of exceptional points (EPs). The real part of the eigenvalues is degenerate along an open-ended contour—the bulk Fermi arc (blue line)—connecting the pair of EPs. (**C**) Examples of the isofrequency contours in this system, including the open bulk Fermi arc at the EP frequency (middle panel), and closed contours at higher (upper panel) or lower (lower panel) frequencies. Solid lines are from the analytical model, and circles are from numerical simulations.

[1]Department of Physics, Massachusetts Institute of Technology, Cambridge, MA 02139, USA. [2]State Key Laboratory of Advanced Optical Communication Systems and Networks, Department of Electronics, Peking University, Beijing 100871, China. [3]Department of Chemistry, Massachusetts Institute of Technology, Cambridge, MA 02139, USA. [4]Department of Applied Physics, Yale University, New Haven, CT 06520, USA. [5]Department of Physics and Astronomy, University of Pennsylvania, Philadelphia, PA 19104, USA.
*These authors contributed equally to this work. †Present address: Department of Physics, Harvard University, Cambridge, MA 02138, USA.
‡Corresponding author. Email: bozhen@sas.upenn.edu

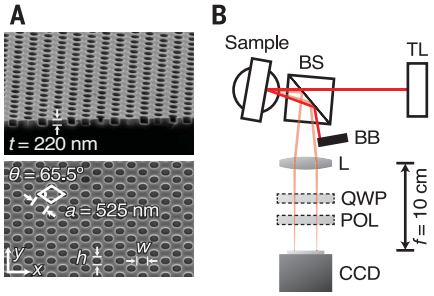

Fig. 2. Fabricated PhC slab and measurement setup. (**A**) SEM images of the PhC samples: side view (top panel) and top view (bottom panel). (**B**) Schematic of the scattering measurement setup. Vertically polarized light from a tunable continuous-wave Ti-Sapphire laser (TL) scatters off the PhC slab and is collected by a CCD camera placed at the focal plane of the lens (L). The specular reflection is blocked to ensure only scattered light is imaged. POL and QWP are used in polarimetry measurements of the scattered light. TL, tunable laser; BS, beam splitter; L, convex lens with 10-cm focal length; QWP, quarter-wave plate; POL, polarizer; BB, beam block.

Our scheme involves splitting a single DP into a pair of EPs, which directly leads to the emergence of a bulk Fermi arc. First, consider a 2D-periodic PhC with a square lattice of circular air holes introduced into a dielectric material. In this Hermitian system (no material gain, loss, or radiation loss), the crystalline symmetry (C_{4v}) ensures a quadratic band degeneracy at the center of the Brillouin zone (*26*). As this C_{4v} symmetry is broken, e.g., by shearing the structure into a rhombic lattice with elliptical holes (Fig. 1A), the quadratic degeneracy point splits into a pair of DPs situated at $(\pm k_D, 0)$ along the k_x axis. The same splitting behavior is shown in both analytical models and numerical simulations (*21*, *26*, *27*).

Next, we consider a non-Hermitian system consisting of a finite-thickness PhC slab (inset of Fig. 1B), where modes near the DP become resonances with finite lifetime because of radiative losses toward the top and bottom. Adopting the even and odd y–mirror-symmetric eigenstates at the DP as basis and taking into account the radiation losses via non-Hermitian perturbations, the effective Hamiltonian in the vicinity of the original DP at $(k_D, 0)$ can be written as (*8*, *21*)

$$H_{\text{eff}} = \omega_D - i\gamma_0 + (v_g\delta k_x - i\gamma)\sigma_z + v_g\delta k_y\sigma_x \quad (1)$$

with complex eigenvalues of

$$\omega_\pm = \omega_D - i\gamma_0 \pm \sqrt{(v_g^2\delta k^2 - \gamma^2) - 2i\gamma v_g\delta k_x} \quad (2)$$

Here, $\sigma_{x,z}$ are Pauli matrices, ω_D is the DP frequency, $(\delta k_x, \delta k_y)$ is the momentum displacement from $(k_D, 0)$, and $\delta k^2 = \delta k_x^2 + \delta k_y^2$. Meanwhile, $\gamma_0 \pm \gamma$ are the radiation decay rates of the even and odd y–mirror-symmetric modes, taking into account that the two modes have different coupling strengths to the continuum; v_g is the group velocity describing the dispersion around the DP, which for simplicity is here chosen to be the same along all directions [see (*26*) for the general case]. The real part of the complex eigenvalues $\omega_\pm$ characterizes the resonance frequency, whereas the imaginary part represents the linewidth of the resonance.

The eigenvalue spectrum exhibits a pair of EPs at $(\delta k_x, \delta k_y) = (0, \pm\gamma/v_g)$, near the original DP, when the square-root term in Eq. 2 vanishes and the two eigenvectors coalesce (Fig. 1B). The existence of such EPs is topologically robust against continuous changes in the Hamiltonian (*8*, *26*) and does not rely on any symmetries or fine-tuning. Furthermore, this pair of EPs is connected in momentum space by an open-ended arc—a bulk Fermi arc, along which the real part of the complex eigenvalues is degenerate at ω_D (Fig. 1C, middle panel). Although sharing features similar to previously studied Fermi arcs—both are open-ended isofrequency contours—our bulk Fermi arc resides at one frequency in the bulk dispersion rather than on the surface of a 3D Hermitian system and originates from non-Hermiticity rather than from the presence of Weyl points. As the frequency ω decreases from above ω_D, the closed isofrequency contour at ω shrinks (Fig. 1C, top panel), eventually turning into the open Fermi arc when $\omega = \omega_D$ (Fig. 1C, middle panel), and expands out again into a closed contour at even lower frequencies (Fig. 1C, bottom panel). Taken together, the band structure around the EPs forms a double–Riemann sheet topology (Fig. 1B). This originates from the complex square-root term in the dispersion in Eq. 2, which, depending on the sign choice of the square root, results in two sheets. The two eigenvalues continuously evolve on each sheet, and their real parts become degenerate along an open-ended curve—the bulk Fermi arc. From a different point of view, this can also be understood as a nodal arc in the bulk band structure, in analogy to nodal lines in semimetal systems (*2*). We further verify the existence of bulk Fermi arcs in realistic PhC slab structures via numerical simulations (Fig. 1C, circles), showing a good agreement with analytical results (Fig. 1C, solid lines) (*26*). The extent of the bulk Fermi arcs can be tuned by engineering the band structure and coupling rates to the continuum.

To experimentally demonstrate the bulk Fermi arc, we use interference lithography to fabricate PhC slabs in Si_3N_4 (refractive index $n = 2.02$, thickness $t = 220$ nm) on top of a silica substrate ($n = 1.46$). The PhC structure consists of rhombic unit cells with side length $a = 525$ nm, unit cell angle $\theta = 65.5°$, and elliptical air holes with long-axis length $w = 348$ nm and short-axis length $h = 257$ nm (*26*). Scanning electron microscope (SEM) images of the fabricated samples are shown in Fig. 2A. The structure is immersed in an optical liquid with refractive index matched to that of the silica substrate to create an up-down symmetric environment.

We performed angle-resolved scattering measurements (setup shown in Fig. 2B) to image isofrequency contours of the sample. The PhC sample is illuminated with a tunable continuous-wave Ti:Sapphire laser that is vertically polarized, while scattered light—arising from natural fabrication imperfections of the sample—is collected with a charge-coupled device (CCD) camera placed at the focal plane of a convex lens with 10-cm focal length. Because of resonant enhancement, the scattered light will have strongest intensity only along directions where the underlying resonances share the same frequency as the pump laser, and thus the isofrequency contours of the sample are directly imaged onto the CCD (*26*, *28*, *29*). Compared to previous measurement techniques based on the reflection spectrum (*13*), this scattering method enables fast and direct extraction of band information, without fitting to any specific models. To show the full shrinking-and-reexpanding feature of the isofrequency contours around the bulk Fermi arc, the laser wavelength is tuned from 794 nm down to 788 nm at steps of ~0.2 nm. Furthermore, the polarization at each point along a given isofrequency contour is determined through polarimetry measurements, by optionally inserting a quarter-wave plate and a polarizer in front of the CCD (*26*).

At a few representative wavelengths around the Fermi arc, the numerical results of isofrequency contours (Fig. 3A) obtained from simulating extracted structural parameters are plotted against the experimental results (Fig. 3B), showing good agreement with each other. Here, for better comparison, the numerical results are offset by 0.5 nm relative to the experiments. [See (*26*) about possible reasons for this wavelength offset and the full set of isofrequency contours measured at different wavelengths.] To focus on the bulk Fermi arc, we highlight the region of interest in both panels, where the isofrequency contours clearly demonstrate the shrinking and reexpanding behavior. As shown in Fig. 3, as the wavelength decreases from 794.0 nm, the corresponding isofrequency contour shrinks (top two rows), and eventually becomes an open-ended arc at 791.0 nm (middle row), consistent with our previous theoretical predictions in Fig. 1C. As the wavelength is further decreased down to 789.5 nm and 788.7 nm, the arc expands out into closed contours again (bottom two rows). The bending feature of the contours is a result of higher-order terms in the band dispersion (*26*). The open contour at 791.0 nm (middle row) is a clear, direct observation of the bulk Fermi arc.

So far, we have shown one direct consequence of the unique double–Riemann sheet topology near paired EPs—the bulk Fermi arc. Next, we demonstrate another consequence: half-integer topological charges in the polarization configuration, which also serve as a direct experimental proof of the $\nu = \pm 1/2$ topological index of an EP. These topological charges describe the direction (clockwise or counterclockwise) and number of times the polarization vector winds around a point or line singularity in the optical field, and in our particular system, we observe a robust

180° winding around the Fermi arc, corresponding to a half-integer topological charge.

To fully reconstruct the far-field polarization configurations of the resonances, we perform polarimetry measurements by recording the intensity of isofrequency contours after passing through six different configurations of polarizers and/or waveplates (*26*). Although the incoming light is vertically polarized, the scattered light at each point along the contour is, in general, elliptically polarized, reflecting the polarization state of its underlying resonance. Taking points X and Z in Fig. 4A as examples: After passing through a vertical polarizer, the scattered light is weak (strong) at point X(Z); whereas after a horizontal polarizer, the relative intensity of the scattered light switches between points X and Z. This clearly shows that the far field of the underlying resonance at point X(Z) is mostly horizontally (vertically) polarized.

Examples of the fully reconstructed spatial polarizations (blue ellipses) at representative points along the 794-nm isofrequency contour (red solid line) are shown in the top panel of Fig. 4B, which agree well with numerical results (Fig. 4B, bottom panel). Furthermore, both experimental and numerical results show 180° winding of the polarization long axis, as illustrated by the green arrows in Fig. 4B: As the momentum point starts from point X, traverses the full contour in the counterclockwise direction, and returns to point X, the polarization long axis flips direction by rotating 180° in the clockwise direction—corresponding to a $-\frac{1}{2}$ topological charge being enclosed in the loop. These results thus indicate that the far-field emission from our PhC is a vector-vortex beam with half-integer topological charge, in stark contrast to the integer vector beams realized in photonic crystal surface–emitting lasers (*24*).

We now explain the fundamental connections between the half-integer topological charges observed in the far-field polarization and the half-integer topological index of an EP (*8*), manifested as its mode-switching property (*26*). Along the k_x axis, the two bands forming the EP pair in our system have orthogonal linear polarizations due to the y–mirror symmetry: One is horizontal (e.g., mode X in Fig. 4C), whereas the other is vertical (e.g., modes Z and W). As we follow a closed path in momentum space X → Y → Z → W that encircles one of the EPs in the counterclockwise direction, the initial eigenstate X (horizontally polarized) on the top sheet adiabatically evolves into state Z (vertically polarized) and eventually into final state W (vertically polarized) on the bottom sheet, owing to the mode-switching topological property of the EP (*10*–*12*). The switching behavior of the eigenmodes—from X to W—directly follows from their eigenvalue swapping behavior on the complex plane (*26*). Equivalently, one complex eigenvalue winds around the other one by half a circle, thus implying that the topological index of an EP is a half-integer. The orthogonal nature between the polarizations at X and Z, arising from the mode-switching property of the EP, guarantees

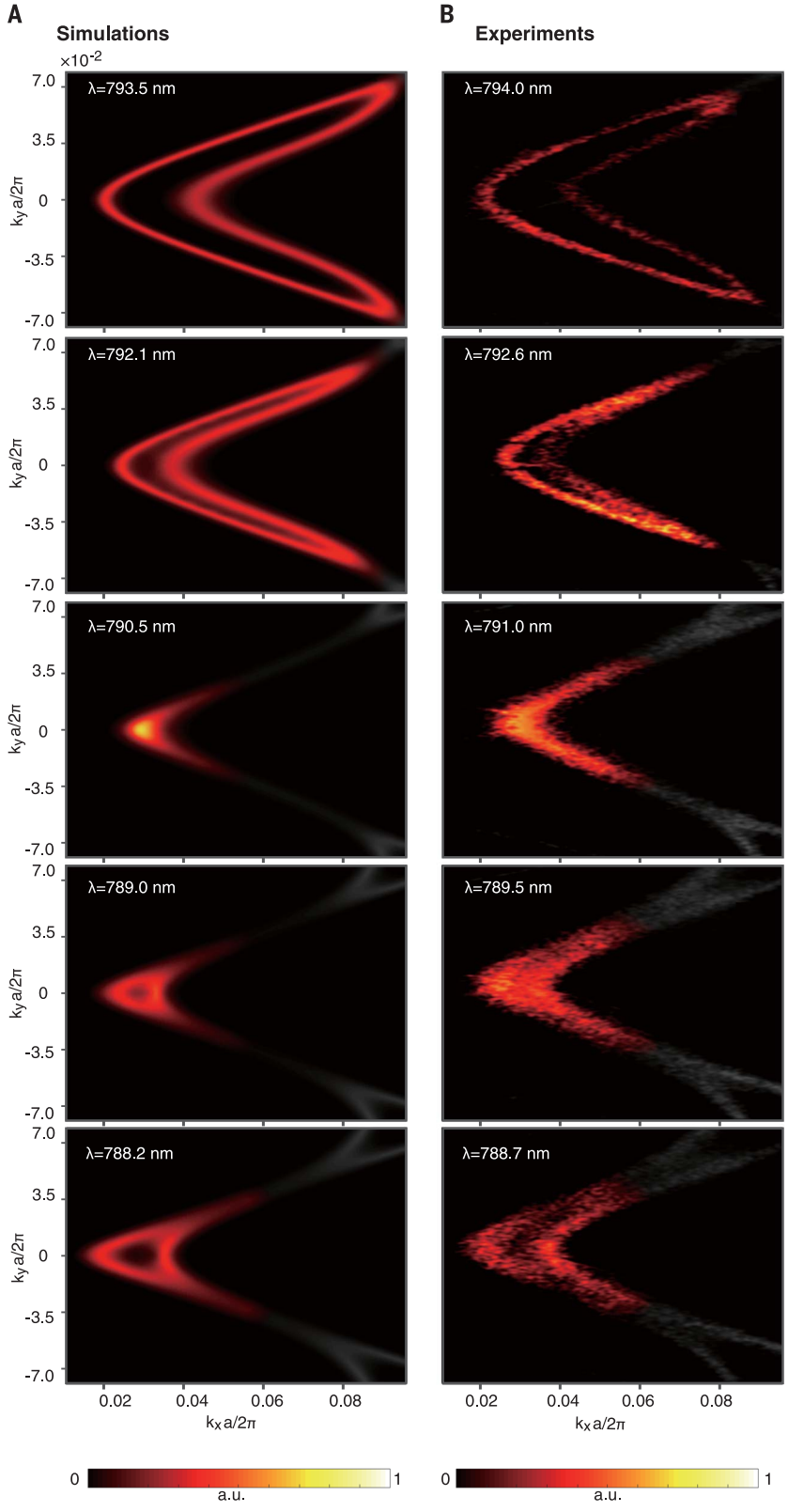

Fig. 3. Experimental demonstration of a bulk Fermi arc. (**A**) Numerically simulated spectral density of states and (**B**) experimentally measured isofrequency contours at five representative wavelengths. The bulk Fermi arc appears at 791.0 nm (middle row), when the isofrequency contour becomes open-ended. The regions of interest are highlighted in all panels to emphasize the shrinking (top two rows) and reexpanding (bottom two rows) feature of isofrequency contours near the bulk Fermi arc. The numerical results are offset by 0.5 nm for better comparison.

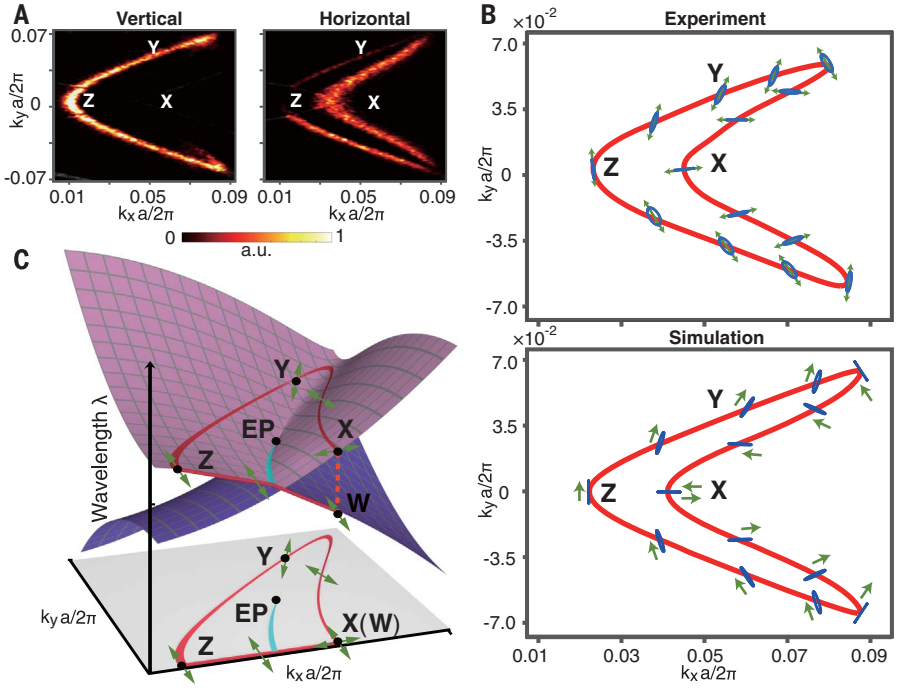

Fig. 4. Experimental demonstration of polarization topological half charges around the bulk Fermi arc. (**A**) Intensity of scattered light at 794 nm after passing through a vertical (horizontal) polarizer is plotted in the left (right) panel, showing that point X(Z) is mostly horizontally (vertically) polarized. (**B**) Experimental reconstruction (top) and numerical simulation (bottom) of the full polarization information, showing the polarization ellipses (blue ellipses) as well as their long-axis directions (green arrows) along an isofrequency contour (red line). As shown by the green arrows in the bottom panel, the polarization long axis exhibits a $-\frac{1}{2}$ topological charge. (**C**) Schematic illustration of the mode switching (X to W) in the band structure, along a loop enclosing an EP (X-Y-Z-W), as a result of the double–Riemann sheet topology. This mode-switching behavior directly leads to the half-integer topological index of an EP and the half-charge polarization winding.

a $(n+\frac{1}{2})\pi$-rotation ($n \in \mathbb{Z}$) of the polarization vector along half the contour. Again using the y–mirror symmetry, the full isofrequency contour will accumulate twice the rotation angle, to a combined $(n+\frac{1}{2}) \times 2\pi$-rotation, corresponding to a half-integer topological charge of $n+\frac{1}{2}$.

We have thus shown the intimate connection between polarization vector winding in singular optics and the double–Riemann sheet topology of paired EPs. Our experimental demonstration—generating half-integer vector-vortex beams directly from the topological properties of EPs—not only distinguishes our study from the previously known integer topological charges of polarization around bound states in the continuum (*30*), but also proves the nontrivial topology of EPs.

We have demonstrated that the topological properties of paired EPs endow the band structure and far-field emission with unique features, manifested as the emergence of bulk Fermi arcs and polarization half topological charges. Our structure also provides an easily realizable method to create half-integer vector-vortex beams (*25*) at a wide range of frequencies. Future prospects leveraging the topological landscape around paired EPs may enable PhC lasers with exotic emission profiles (*24*), such as twisted Möbius strips. The isolated EPs found in our structure also provide a straightforward platform for studying the influence of EPs and their topology on light-matter interactions, such as modified Purcell factors for spontaneous emission enhancement and nonlinear optics generation. Our observation of bulk Fermi arcs and polarization half charges extends the existing framework of topological physics in closed systems into a new regime involving open systems and provides a platform for the future exploration of non-Hermitian topological physics in general wave systems, ranging from photonic and acoustic to electronic and polaritonic systems.

REFERENCES AND NOTES

1. A. H. Castro Neto, F. Guinea, N. M. R. Peres, K. S. Novoselov, A. K. Geim, *Rev. Mod. Phys.* **81**, 109–162 (2009).
2. N. P. Armitage, E. J. Mele, A. Vishwanath, *Rev. Mod. Phys.* **90**, 015001 (2018).
3. M. Hasan, C. Kane, *Rev. Mod. Phys.* **82**, 3045–3067 (2010).
4. X. L. Qi, S. C. Zhang, *Rev. Mod. Phys.* **83**, 1057–1110 (2011).
5. L. Lu, J. D. Joannopoulos, M. Soljačić, *Nat. Photonics* **8**, 821–829 (2014).
6. N. Moiseyev, *Non-Hermitian Quantum Mechanics* (Cambridge Univ. Press, 2011).
7. D. Leykam, K. Y. Bliokh, C. Huang, Y. D. Chong, F. Nori, *Phys. Rev. Lett.* **118**, 040401 (2017).
8. H. Shen, B. Zhen, L. Fu, arXiv:1706.07435 [cond-mat.mes-hall] (22 June 2017).
9. W. D. Heiss, *J. Phys. Math. Gen.* **45**, 444016 (2012).
10. C. Dembowski *et al.*, *Phys. Rev. Lett.* **86**, 787–790 (2001).
11. J. Doppler *et al.*, *Nature* **537**, 76–79 (2016).
12. H. Xu, D. Mason, L. Jiang, J. G. E. Harris, *Nature* **537**, 80–83 (2016).
13. B. Zhen *et al.*, *Nature* **525**, 354–358 (2015).
14. Z. Lin *et al.*, *Phys. Rev. Lett.* **106**, 213901 (2011).
15. C. M. Bender, S. Boettcher, *Phys. Rev. Lett.* **80**, 5243–5246 (1998).
16. H. Hodaei *et al.*, *Nature* **548**, 187–191 (2017).
17. W. Chen, Ş. Kaya Özdemir, G. Zhao, J. Wiersig, L. Yang, *Nature* **548**, 192–196 (2017).
18. H. Hodaei, M.-A. Miri, M. Heinrich, D. N. Christodoulides, M. Khajavikhan, *Science* **346**, 975–978 (2014).
19. L. Feng, Z. J. Wong, R.-M. Ma, Y. Wang, X. Zhang, *Science* **346**, 972–975 (2014).
20. O. N. Kirillov, A. A. Mailybaev, A. P. Seyranian, *J. Phys. Math. Gen.* **38**, 5531–5546 (2005).
21. H. Zhou, "Tailoring light with photonic crystal slabs: From directional emission to topological half charges," thesis, Massachusetts Institute of Technology (2016).
22. V. Kozii, L. Fu, arXiv:1708.05841 [cond-mat.mes-hall] (19 August 2017).
23. M. V. Berry, M. R. Dennis, *Proc. R. Soc. A Math. Phys. Eng. Sci.* **459**, 1261–1292 (2003).
24. E. Miyai *et al.*, *Nature* **441**, 946 (2006).
25. T. Bauer *et al.*, *Science* **347**, 964–966 (2015).
26. See supplementary materials.
27. Y. D. Chong, X.-G. Wen, M. Soljačić, *Phys. Rev. B* **77**, 235125 (2008).
28. E. C. Regan *et al.*, *Sci. Adv.* **2**, e1601591 (2016).
29. L. Shi, H. Yin, X. Zhu, X. Liu, J. Zi, *Appl. Phys. Lett.* **97**, 251111 (2010).
30. B. Zhen, C. W. Hsu, L. Lu, A. D. Stone, M. Soljačić, *Phys. Rev. Lett.* **113**, 257401 (2014).

ACKNOWLEDGMENTS

We thank T. Savas for fabrication of the samples. We also thank S. Johnson, E. Mele, L. Lu, Y. Shen, S. Skirlo, S. Liu, J. Y. Lee, F. Machado, N. Rivera, G. Zhang, and S. Moore for helpful discussions. Research was supported in part by the Army Research Office through the Institute for Soldier Nanotechnologies under contract no. W911NF-13-D-0001 [photon management for developing nuclear-thermophotovoltaic (TPV) and fuel-TPV mm-scale systems]. Research was also supported as part of the S3TEC, an Energy Frontier Research Center funded by the U.S. Department of Energy under grant no. DE-SC0001299 (for fundamental photon transport related to solar TPVs and solar thermoelectrics), and by the Air Force Research Lab under contract FA8650-16-D-5403. H.Z. acknowledges support from the Undergraduate Research Opportunities Program at Massachusetts Institute of Technology. B.Z. acknowledges the Air Force Office of Scientific Research Young Investigator Program under award number FA9550-18-1-0133. C.P. acknowledges support from the National Natural Science Foundation of China under grant nos. 61575002 and 61320106001, and the China Scholarship Council. C.W.H. acknowledges support from the National Science Foundation under grant NSF DMR-1307632. Y.Y. and K.A.N. were supported in part by Skoltech as part of the Skoltech Next Generation Program. H.Z. and B.Z. conceived the idea. H.Z. performed the analytical calculations and numerical simulations. H.Z., B.Z., C.P., and Y.Y. conducted the experiments and analyzed the data. H.Z. and B.Z. wrote the manuscript, with input from all authors. B.Z., M.S., and J.D.J. supervised the research. All authors contributed to the analysis and discussion of the results. All data needed to evaluate the conclusions are present in the paper and/or the supplementary materials. Additional data related to this paper may be requested from the authors.

SUPPLEMENTARY MATERIALS

www.sciencemag.org/content/359/6379/1009/suppl/DC1
Supplementary Text
Figs. S1 to S4
References (*31*–*38*)
Movie S1

17 September 2017; accepted 19 December 2017
Published online 11 January 2018
10.1126/science.aap9859

Science

Observation of bulk Fermi arc and polarization half charge from paired exceptional points

Hengyun Zhou, Chao Peng, Yoseob Yoon, Chia Wei Hsu, Keith A. Nelson, Liang Fu, John D. Joannopoulos, Marin Soljacic and Bo Zhen

Science **359** (6379), 1009-1012.
DOI: 10.1126/science.aap9859originally published online January 11, 2018

Exploring photonic topology

Scattering topological effects are being explored in a variety of electronic and optical materials systems owing to their robustness against defects (see the Perspective by Özdemir). Yang *et al.* designed and fabricated an ideal optical analog of a three-dimensional Weyl system. Angular transmission measurements revealed four Weyl points at the same energy, as well as the signature helicoidal arcs associated with such an exotic topological system. Zhou *et al.* theoretically proposed and experimentally demonstrated the formation of a topologically protected bulk Fermi arc. They attributed the formation of the arc to the topological nature of paired exceptional points (points at which gain and loss in the system are matched). Photonic crystals may provide a powerful platform for studying exotic properties of topological electronic systems and may also be used to develop optical devices that exploit topological properties of light-matter interactions.

Science, this issue p. 1013, p. 1009; see also p. 995

Science (print ISSN 0036-8075; online ISSN 1095-9203) is published by the American Association for the Advancement of Science, 1200 New York Avenue NW, Washington, DC 20005. The title *Science* is a registered trademark of AAAS.